

Unravelling the role of phoretic and hydrodynamic interactions in active colloidal suspensions

A. Scagliarini¹ and I. Pagonabarraga²

¹*IAC-CNR, Istituto per le Applicazioni del Calcolo “Mauro Picone”,
Via dei Taurini 19, 00185 Rome, Italy. E-mail: andrea.scagliarini@cnr.it*

²*CECAM, Centre Européen de Calcul Atomique et Moléculaire,
Ecole Polytechnique Fédérale de Lausanne, Batochimie, Avenue Forel 2, 1015 Lausanne, Switzerland*

Active fluids comprise a variety of systems composed of elements immersed in a fluid environment which can convert some form of energy into directed motion; as such they are intrinsically out-of-equilibrium in the absence of any external forcing. A fundamental problem in the physics of active matter concerns the understanding of how the characteristics of the autonomous propulsion and agent-agent interactions determine the collective dynamics of the system. We study numerically suspensions of self-propelled diffusiophoretic colloids, in (quasi)-2d configurations, accounting for both dynamically resolved solute-mediated phoretic interactions and solvent-mediated hydrodynamic interactions. Our results show that the system displays different scenarios at changing the colloid-solute affinity and it develops a cluster phase in the chemoattractive case. We study the statistics of cluster sizes and cluster morphologies for different magnitudes of colloidal activity. Finally, we provide evidences that hydrodynamics plays a relevant role in the aggregation kinetics and cluster morphology, significantly hindering the cluster growth.

I. INTRODUCTION

Collective behaviour is widespread in Nature: fish schools, insects swarms, bacterial colonies, plankton blooms are but a few instances of it. Collective phenomena in Active Matter are characterized by long-ranged correlations and large density fluctuations [1, 2], complex pattern-formation [3], and non-equilibrium changes of state, such as a flocking [4–6], clustering [7], or mobility induced phase separation [8, 9]. Answering key questions on how individuals interact and communicate goes even beyond fundamental goal of unravelling the physical mechanisms at the basis of self-organisation in living systems. It will help the design of micro- and nano-scale self-propelled objects [10–17], with the aim of generating motion in miniaturized devices and developing biomimetic environments [18–21]. Despite most of these natural and artificial particles displace in a fluid medium, the role played by particle-motion induced hydrodynamic correlations has been essentially overlooked so far. Here we present a numerical study of a suspension of non-Brownian colloids which move responding to gradients of a self-generated concentration field [22–25]; the latter determines, dynamically by diffusion and advection, a means of interaction/communication among the active particles. In analogy to typical experimental setups [9, 26–29], we consider the dynamics of a layer of self-propelled colloids (SPCs) on a flat wall under the action of gravity embedded in a liquid medium. We find that the system develops two distinct dynamic regimes, forming large scale clusters when the interaction of the colloidal particles with solute is of “chemoattractive” type. We characterize the transition between the two observed non-equilibrium regimes and focus on the morphology and dynamics of the cluster phase. With respect to previous studies, we single out quantitatively,

for the first time, the impact of solvent hydrodynamics on the collective dynamics of suspensions of active self-diffusiophoretic Janus colloids.

II. THEORY AND NUMERICAL MODEL

The 3d Navier-Stokes equations for the fluid (solvent + solute) velocity field \mathbf{u} and for the solute concentration field c , which read

$$\begin{aligned}\partial_t \mathbf{u} + \nabla \cdot (\mathbf{u}\mathbf{u}) &= -\frac{1}{\rho_f} \nabla P + \nu \nabla^2 \mathbf{u} \\ \partial_t c + \nabla \cdot (\mathbf{u}c) &= D \nabla^2 c + \mathcal{Q}_c - k_d c,\end{aligned}\quad (1)$$

are integrated by means of a hybrid lattice Boltzmann (LB)/finite difference method [30–35]. Here, ρ_f is the fluid density (assumed to be constant, since the flow regime is close to incompressible, the maximum Mach number being $Ma \approx 10^{-2}$), P is the pressure field, ν and D are, respectively, the kinematic viscosity and the scalar field diffusivity. \mathcal{Q}_c represents the production of solute by the colloids and it is non-zero only at particle surfaces. The local sink term $-k_d c$ models the degradation of products with rate k_d (with associated characteristic screening length $\ell_d = \sqrt{\frac{D}{k_d}}$ of approximately eight times the particle radius). The velocities attained in our simulations are such that the typical particle Reynolds $Re = V_p R / \nu$ and Péclet $Pe = V_p R / D$ numbers are always smaller than 10^{-1} (V_p is the self-propulsion speed), thus making the advection terms in (1) negligible. The fluid is confined along the z -direction by two parallel walls (distant about 10 colloid radii), at which a no-slip boundary condition is imposed on the velocity field and a zero-flux condition applies for the equation for c ; the system is periodic in x, y . Colloids are described as solid spheres of radius R ,

mass M and moment of inertia $I = \frac{2}{5}MR^2$, at whose surfaces momentum and torque exchange between particle and fluid is implemented via the bounce-back-on-links scheme for LB probability densities [36–39]. This entails a force \mathbf{F}_h and a torque \mathbf{T}_h , exerted by the fluid on the particle and resulting from the integrated hydrodynamic stresses over the particle surface, that depend on the global configuration of the velocity field \mathbf{u} ; therefore, \mathbf{F}_h and \mathbf{T}_h mediate also, in the general case, hydrodynamic interactions among particles. According to the theory of colloidal phoresis [40], the interaction with a surrounding non-homogeneous concentration field c induces a flow due to the solute imbalance around the particle surface. This flow, though, is confined to a layer much thinner than the particle size, since the interaction is typically very short-ranged; consequently, a lubrication theory analysis leads to account for it as an effective boundary condition between the inner layer and the outer fluid, resulting in the following effective slip velocity for the fluid velocity \mathbf{u} at the particle surface Σ :

$$\mathbf{v}_s = \mu(\mathbf{r}_S)(\mathbf{1} - \hat{\mathbf{r}}_S \otimes \hat{\mathbf{r}}_S) \cdot \nabla c, \quad (2)$$

where the *phoretic mobility* $\mu(\mathbf{r}_S)$, $\mathbf{r}_S \in \Sigma$, contains the details of the colloid-solute interaction. This formulation paves the way, then, to a multi-scale modelling approach where fluid dynamic processes localised (on molecular scales) close to the particle (and embedded in the solute-gradient-dependent slip velocity) are effectively decoupled from large scale flows in the solvent and associated long-range hydrodynamic interactions. Introducing (2) in the bounce-back-on-links algorithm [36–39] effectively amounts to imposing a phoretic force \mathbf{F}_p and torque \mathbf{T}_p on the particle that take the form:

$$\begin{aligned} \mathbf{F}_p &= -\frac{M}{(4\pi R^2)\tau_S} \int \int_{\Sigma} \mathbf{v}_s(\mathbf{r}_S) d\mathbf{r}_S \\ \mathbf{T}_p &= -\frac{3I}{(8\pi R^3)\tau_S} \int \int_{\Sigma} \hat{\mathbf{n}}(\mathbf{r}_S) \wedge \mathbf{v}_s(\mathbf{r}_S) d\mathbf{r}_S, \end{aligned} \quad (3)$$

where $\hat{\mathbf{n}}$ is the outward normal to the sphere (i.e., with reference to figure 1, is the direction of $\frac{\mathbf{r}_S - \mathbf{X}}{|\mathbf{r}_S - \mathbf{X}|}$) and τ_S is the particle Stokes time. For constant phoretic mobility $\mu(\mathbf{r}_S) \equiv \mu$, the particle moves with a net propulsion velocity $\mathbf{V}_p \sim -\mu \nabla c$, directed towards regions of high concentration of solute for negative μ (“chemoattractant”), and escaping from it for positive μ (“chemorepellent”). Each particle produces solute c at a constant rate per unit surface, α_0 , according to the activity profile:

$$\alpha(\mathbf{r}_S) = \begin{cases} \alpha_0 & \text{if } \hat{\mathbf{m}} \cdot \hat{\mathbf{n}} \leq 0 \\ 0 & \text{if } \hat{\mathbf{m}} \cdot \hat{\mathbf{n}} > 0, \end{cases}$$

$\hat{\mathbf{m}}$ being the particle characteristic unit vector (see the sketch in figure 1); although this particular $\alpha(\mathbf{r}_S)$ specifies *Janus*-like particles [41], in principle the numerical scheme can deal with arbitrarily *patchy* [42] active colloids. We stress, furthermore, that the formalism is not specific for self-diffusiophoresis: the only two required ingredients are, in fact, the production of a diffusing scalar

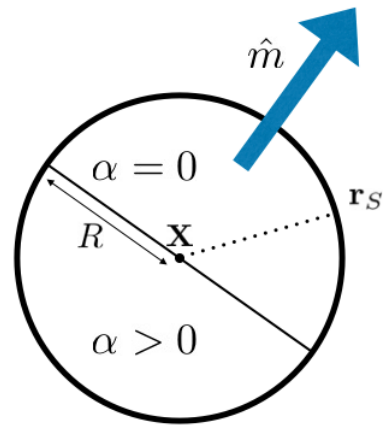


FIG. 1. Sketch of a spherical self-phoretic colloid of radius R . \mathbf{X} is the position of the centre of mass $\hat{\mathbf{m}}$ is the particle characteristic vector, based on which we set the activity profile: $\alpha(\mathbf{r}_S) = \alpha_0$ on the bottom hemisphere ($\hat{\mathbf{m}} \cdot \hat{\mathbf{n}} < 0$) and $\alpha(\mathbf{r}_S) = 0$ on top ($\hat{\mathbf{m}} \cdot \hat{\mathbf{n}} > 0$).

field and a regime of linear response of particles to gradients, and as such it enjoys a wider range of applicability, including systems like thermophoretic colloids [43–45], autochemotactic swimmers [46, 47], gliding bacteria [48, 49]. The Lagrangian dynamics for the position $\mathbf{X}^{(i)}$ and velocity $\mathbf{V}^{(i)}$ of the centre of mass of the i -th SPC ($i = 1, 2, \dots, N$), and for its intrinsic orientation $\hat{\mathbf{m}}^{(i)}$ and angular velocity $\Omega^{(i)}$, is described by the following equations of motion:

$$\begin{aligned} \dot{\mathbf{X}}^{(i)} &= \mathbf{V}^{(i)} \\ \dot{\mathbf{V}}^{(i)} &= \frac{1}{M} (\mathbf{F}_h + \mathbf{F}_p + \mathbf{F}_b) \\ \dot{\hat{\mathbf{m}}}^{(i)} &= \Omega^{(i)} \wedge \hat{\mathbf{m}}^{(i)} \\ \dot{\Omega}^{(i)} &= \frac{1}{I} (\mathbf{T}_h + \mathbf{T}_p), \end{aligned} \quad (4)$$

where \mathbf{F}_b is a generic body force (e.g. gravity) and the hydrodynamic force \mathbf{F}_h and torque \mathbf{T}_h , as well as the force \mathbf{F}_p and torque \mathbf{T}_p stemming from the phoretic mechanism, have been previously introduced. Equations (4) are solved by a standard leap-frog algorithm. An isolated free Janus SPC evolving according to (4) will perform a rectilinear motion with constant speed $V_p = |\mu|\alpha_0/(4D)$ [22, 23, 50]. When assessing the dynamics where no hydrodynamic interactions are present (see section III C), we consider only the equation for c in (1), with $\mathbf{u} \equiv 0$, whereas \mathbf{F}_h and \mathbf{T}_h reduce to the usual translational and rotational frictional drag, respectively. For particles close to contact, lubrication corrections are introduced: the forces and torques acting on two particles approaching each other are calculated, in terms of particle velocities and angular velocities, according to a grand-resistance-matrix formulation [39, 51, 52]. In particular, the lubrication correction takes the form of the difference between the lubrication force at a surface separation h and the force at a given cut-off separation h_c ;

for two particles of radii R_1 and R_2 (the particle-wall interaction corresponds to the limit $R_2 \rightarrow \infty$) this reads [39]:

$$\mathbf{F}_{\text{lub}}(h) = \begin{cases} -6\pi\eta \frac{R_1^2 R_2^2}{(R_1 + R_2)^2} \left(\frac{1}{h} - \frac{1}{h_c} \right) \mathbf{V}_{12} \cdot \hat{\mathbf{r}}_{12} & \text{if } h \leq h_c \\ 0 & \text{if } h > h_c \end{cases} \quad (5)$$

where $\mathbf{r}_{12} = \mathbf{X}_1 - \mathbf{X}_2 \equiv r_{12}\hat{\mathbf{r}}_{12}$ is the particle center-center distance vector and $h = r_{12} - R_1 - R_2$; the cutoff distance is chosen to be $h_c = 0.67$ lattice units, which is an optimal value to get good agreement with lubrication theory calculations, as shown in [39]. Lubrication forces may not be enough, though, to prevent particle overlap (as recognized also in [53, 54]), especially when the particle density is large (even just locally, as, for instance, inside clusters). Therefore, we add also a short-range soft-sphere repulsion modelled by the force $\mathbf{F}_{\text{ss}} \propto (h_c^{ss}/h)^3 - 1$, with cutoff (coinciding with the soft-sphere radius) $h_c^{ss} = 2h_c$.

We have performed numerical simulations of suspensions with $N = 6400$ SPCs on lattices of $1024 \times 1024 \times 24$ grid points ($\approx 410 R \times 410 R \times 10 R$, corresponding to $R = 2.5$ lattice spacings, a value which is relatively small, such to allow simulations of many particle systems, but large enough to keep deviations from the expected physical behaviour, in terms, e.g., of the drag coefficient, below 10% [37, 51]), at fixed area fraction $\phi \approx 0.12$. Particles are subjected to a gravity force \mathbf{F}_b strong enough to prevent them from leaving the bottom wall (the limit fall velocity being five times larger than the self-propulsion speed corresponding to the maximum phoretic mobility considered, i.e. $\frac{F_b}{6\pi\nu\rho_f R} \approx 5 \frac{|\mu|\alpha}{4D}$). A hard-core particle-particle repulsion was introduced to prevent overlapping. Initially particles were randomly distributed on the surface of the bottom wall. Each run lasted approximately $T_{\text{run}} \approx 5800 \tau$. It is worth noticing that, upon proper non-dimensionalisation by the corresponding τ ($\sim 1 s$), T_{run} is comparable with experimental times [9, 26].

III. RESULTS AND DISCUSSION

A. Dynamic scenarios controlled by the phoretic mobility.

A number of experimental and numerical/theoretical studies of self-propelled particles in (quasi)- $2d$ have given indication of the emergence of clustering [9, 26–28, 55–57], however the nature of the mechanisms determining the formation of aggregates lacks a consensual agreement and seems to be strongly system-dependent (see also [16] for a recent review). In our simulations solvent and solute hydrodynamics is fully resolved, from the far field down to distances of the order of the particle size (below which it is regularised by the lubrication interaction). We deal with spherical particles, which rules out the possibility of alignment-induced collective motion; instead, chemi-

cal production and diffusion mediate an effective interaction, analogously to the experimental system studied in [26, 28]. While in the experiments it was surmised that active colloids felt an attractive interaction, here we can tune the affinity of the particles for the solute via the phoretic mobility μ , which can be regarded as an effective charge [58], i.e. positive/negative values induce repulsive/attractive interactions, respectively. Indeed, while for $\mu < 0$ our simulations confirm the formation of clusters, for $\mu > 0$ such cluster phase disappears, with the average cluster size going to zero. Incidentally, let us remark that, in some respect, suspensions of SPCs may recall other systems of interacting microswimmers, as, for instance, attractive squirmers [59]; there are however at least two major differences: for SPCs, unlike squirmers, the characteristic self-propulsion speed is constant only for an isolated swimmer, but in general it depends on the concentration field; the second and probably most important one, from the point of view of collective dynamics, is that while in the squirmer case particle-particle interactions are *frozen* (i.e. dictated by the interaction potential once for all), in a SPCs suspension phoretic interactions are mediated by the solute field and are, therefore, *dynamical*, in the sense that they depend on the *local* (in space and time) field configuration. In other words, phoretic interactions are not pairwise additive but change as a function of the global dynamics, and as such, they give rise to a collective behaviour that is genuinely out-of-equilibrium. In what follows, values of μ will be expressed in units of μ_0 , the absolute phoretic mobility for which an isolated particle of radius R would have unitary Péclet number. To address the impact of the chemical affinity on the collective dynamics quantitatively, we have performed a Voronoi tessellation analysis of the particle space configurations [60, 61] [62].

The bottom insets of Fig.2 show the Voronoi diagrams both for the repulsive and cluster-forming regimes; as clearly visible to the naked eye, the geometries of the Voronoi cells for chemoattractive and chemorepellent active colloids are distinctively different. The standard deviation of the cell area distribution $\sigma_S^2(t) \equiv \frac{1}{N^2} \sum_{i=1}^N (\mathcal{S}_i - \bar{\mathcal{S}})^2$ (normalized by the square of the mean value $\bar{\mathcal{S}}$) turns out to be a good indicator to distinguish the two types of dynamics. In the top inset of Fig. 2 we plot $\sigma_S(t)$, as function of time (given in units of $\tau = R/V_p$, i.e. the time an isolated particle takes to displace by one radius), for two cases with different sign of the phoretic mobility. In the attractive case, $\mu < 0$, cluster formation induces the appearance of very small (and large) cells and, hence, the surface fluctuations grow and eventually saturate at long times. For positive μ , instead, colloids repel each other and tend to reach an optimal covering of the space, implying that $\sigma_S^2(t)$ attains a (lower) value which remains constant in time. Correspondingly, the dependence of $\overline{\sigma_S^2}^{(SS)}$ (the time average of $\sigma_S^2(t)$ over the steady state) on μ discriminates between the two regimes: it is high for negatively large μ ,

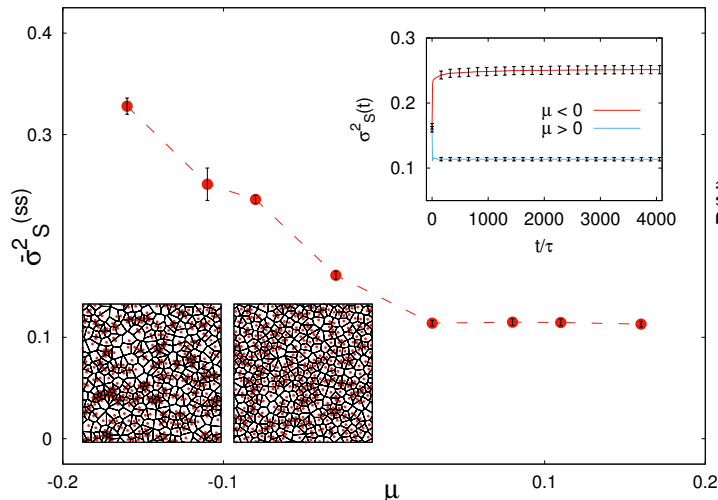


FIG. 2. MAIN PANEL: Steady state standard deviation of Voronoi cell areas as function of the “coupling constant” (the phoretic mobility) μ . TOP INSET: $\sigma_S^2(t)$ vs time for two cases with positive and negative μ . BOTTOM INSETS: Snapshots of the colloid distributions and relative Voronoi diagrams in the attractive, $\mu = -0.11$ (LEFT), and repulsive, $\mu = +0.11$ (RIGHT), case, respectively.

decreases as μ approaches zero and then stays low and constant for $\mu > 0$.

We will focus, in what follows, on the chemoattractive case, but before moving on we stress that the phase diagram for chemorepulsive self-phoretic colloids, as recently shown theoretically and numerically [63, 64], is indeed rather complex and deserves further investigation.

B. Cluster statistics and morphology.

We first characterize the cluster size distribution of chemoattractive SPCs at changing the colloid/solute coupling intensity, $|\mu|$. We identify clusters according to a distance criterion. Two particles share a *bond* if their centers are at a distance equal to or less than a cutoff apart [65], and we define as clusters, groups of particles connected to each other through a bond. We compute probability density functions (PDFs) of cluster sizes over the steady state of each run. Fig. 3 shows such PDFs, which can be in all cases fitted to an exponential, $\mathcal{P}(n) \propto e^{-n/n_c}$, over a wide range of sizes n . The characteristic value n_c and the mean size $\bar{n} = \frac{1}{N_{clus}} \sum_{i=1}^{N_{clus}} n_i$ increase linearly with $|\mu|$ (see inset of figure 3), hence with the velocity of an isolated particle, in agreement with experimental and numerical observations [9, 26, 57]. The global attractor for the SPCs dynamics is a set $\mathcal{S} = \bigcup_{i=1}^{N_{clus}} \mathcal{C}_i$, where \mathcal{C}_i is the i -th cluster with surface of area \mathcal{A}_i and containing n_i SPCs. Correspondingly, the colloid number density becomes $\rho(x) = \rho_i = n_i/\mathcal{A}_i$ if

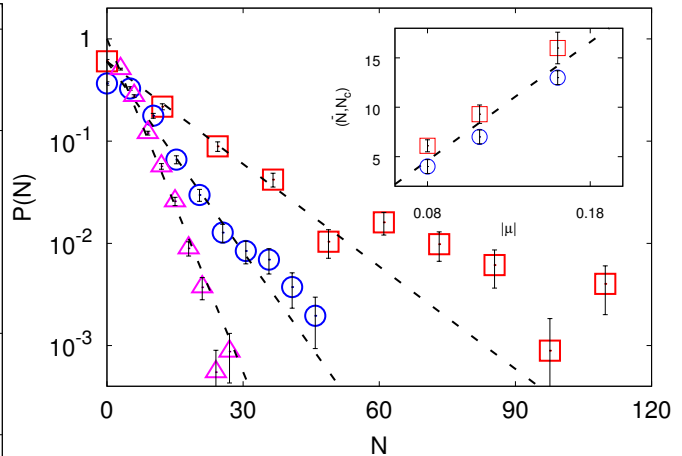


FIG. 3. MAIN PANEL: PDFs of cluster sizes for three values of the phoretic mobility: $\mu = -0.16$ (\square), $\mu = -0.11$ (\circ) and $\mu = -0.08$ (\triangle); the dashed lines represent exponential fit which are drawn to guide the eye. INSET: Characteristic (n_c , \circ) and mean (\bar{n} , \square) cluster sizes as function of $|\mu| \propto V_p$, the intrinsic SPC velocity (the dashed line indicates a linear relation).

$x \in \mathcal{C}_i$ and zero otherwise. Since the colloid density fluctuations can be expressed as $\sigma_\rho^2 = \langle (\rho(x) - \langle \rho \rangle)^2 \rangle$ (where $\langle \dots \rangle$ denotes a surface average), we arrive at

$$\sigma_\rho^2 \propto \langle \rho(x)^2 \rangle = \sum_{i=1}^{N_{clus}} \frac{\rho_i^2 \mathcal{A}_i}{|\Sigma|} \mathcal{P}(\mathcal{A}_i), \quad (6)$$

where $|\Sigma|$ is the measure of the whole plane, and $\mathcal{P}(\mathcal{A}_i)$ is the probability of having a cluster of area \mathcal{A}_i . The number of particles in a cluster n is known to scale with the cluster gyration radius R_g as $n \sim R_g^{d_f}$, d_f being the fractal (Hausdorff) dimension [66, 67]; hence, the density of the i -th cluster, ρ_i , will behave as $\rho_i \sim \mathcal{A}_i^{d_f/2-1}$. The exponential behavior of $\mathcal{P}(n)$ predicts that

$$\sigma_\rho^2 \sim \sigma_{\rho_0}^2 (1 + a|\mu|)^{\zeta(d_f)}, \quad \zeta(d_f) = \frac{3d_f - 2}{d_f}, \quad (7)$$

where $\sigma_{\rho_0}^2$ stands for the fluctuations for a inactive particles and a is a phenomenological parameter, and where we have used the relation $n_c \sim |\mu|$ [68] (see inset of figure 3). Fig. 4 shows the quantitative agreement of the predicted power law, with the correct scaling exponent, with the numerical observations.

C. Role of hydrodynamic interactions.

Self-propelled colloids interact due to both the chemicals they produce and the flows they induce. Understanding the relative magnitude and competition between these two sources of dynamic interactions remains

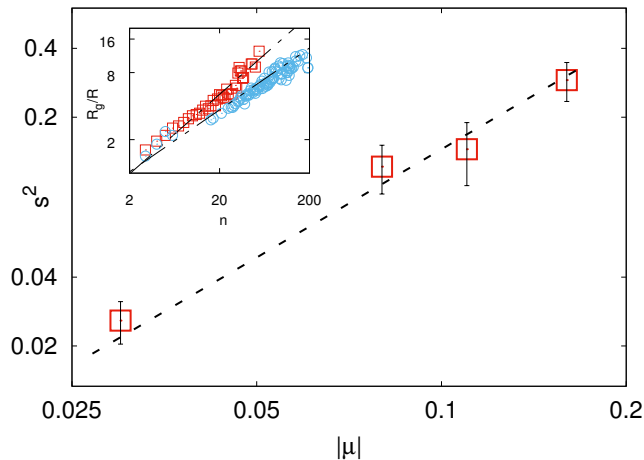


FIG. 4. MAIN PANEL: Deviation of the steady state SPC density fluctuations σ_ρ^2 from the value for inactive particles $\sigma_{\rho_0}^2$, normalized as $s^2 = \frac{\sigma_\rho^2 - \sigma_{\rho_0}^2}{\sigma_{\rho_0}^2 - \langle \rho \rangle^2}$, vs the coupling strength $|\mu|$ from LB (squares) and the phenomenological derivation (7), with fractal dimension $d_f = 1.4$, as measured in the simulations. INSET: Mean gyration radius of clusters vs number of particles with (\square) and without (\circ) HI. The two dashed lines represent the power law $R_g \sim n^{1/d_f}$ ($d_f = 1.8$ for no-HI).

challenging. As described in section II, the model put forward allows us to switch off the hydrodynamic interactions (HI), yet keeping the self-phoretic mechanism and the correct translational and rotational hydrodynamic friction. Interestingly, our study reveals that, although the different dynamic scenarios at changing the sign of the phoretic mobility are preserved even without HI (being mainly determined by the chemical interaction), HI have a profound effect in the kinetics of formation and morphology of the observed aggregates. In the absence of particle induced flows in the solvent, attractive SPCs ($\mu < 0$) show an enhanced tendency to form clusters, as it appears in figure Fig. 5, where we compare the time evolution of the mean cluster size $\bar{n}(t)$, with and without HI (no-HI). In the no-HI case, clusters coarsen, with $\bar{n}(t)$ growing in time as $t^{1/2}$ (top right inset), as for domains in a spinodal decomposition. The same behaviour ($\bar{n}(t) \sim t^{1/2}$) has been observed, indeed, in simulations of self-propelled Brownian particles interacting via a shifted-truncated Lennard-Jones potential [56, 59]. With HI, instead, coarsening is arrested, as observed in experiments [26]. Simulations have suggested that in suspensions of attractive squirmers the emergence of continuous or arrested coarsening is selected depending on the form and intensity of the active stress (the coefficient B_2 in the squirmer terminology) [59]; self-phoretic Janus colloids behave, in this respect, as squirmers with $B_2 = 0$ [69], for which, indeed, arrested coarsening was observed [59]. Due to the non stationarity of the coarsening pro-

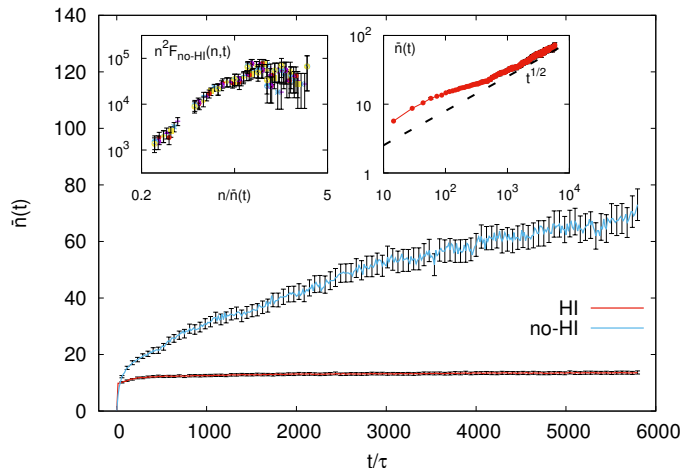


FIG. 5. MAIN PANEL: Mean cluster size \bar{n} vs time from simulations with (HI) and without (no-HI) hydrodynamic interactions (the values for the HI case are magnified by a factor two, for the sake of clarity of visualisation). LEFT INSET: Cluster size distributions for $\mu = -0.16$ and no-HI, at various times $t \in [1500\tau; 3000\tau]$ during the coarsening process. RIGHT INSET: Log-log plot of \bar{n} vs t , without HI, highlighting the scaling $t^{1/2}$ in the coarsening process.

cess, steady state PDFs of cluster sizes cannot be computed in the no-HI simulations. Nevertheless, we observe that instantaneous cluster size distributions $F(n, t)$ (i.e. the number of clusters of size n at time t) tend to assume a self-preserving scaling form $F(n, t) \sim n^{-2} f(n/\bar{n}(t))$, as it happens in classical colloidal aggregation phenomena for mass-conserving systems [70]. This is shown in the top left inset of Fig. 5, where we plot $n^2 F(n, t)$ vs $n/\bar{n}(t)$ and see that all sets of points for different t 's in the coarsening regime where $\bar{n} \sim t^{1/2}$, within error bars, collapse onto each other. The statement on the different dynamics, with and without HI, is corroborated by the inspection of the radial distribution functions (RDFs) [71] (indicated as $g_{HI}(r, t)$ and $g_{no-HI}(r, t)$, respectively), defined as the probability of finding a particle between the distances r and $r + dr$ from a reference particle (and averaged over all particles), i.e.

$$g(r, t) = \frac{1}{\rho_N N} \sum_{i=1}^N \sum_{\substack{j=1 \\ j \neq i}}^N \delta(\mathbf{r} - \mathbf{X}_j(t) + \mathbf{X}_i(t)),$$

where ρ_N is the particle number density and $\delta(x)$ is the Dirac's delta. RDFs at different times are shown in Fig. 6: without HI the peaks are higher and decay more slowly, associated to the development of clusters larger than those formed when hydrodynamics is active. Besides, clusters appear substantially more compact, as appreciated in the snapshots (insets) and quantified by the measurement of a larger fractal dimension ($d_f^{(HI)} \approx 1.4$ and $d_f^{(no-HI)} \approx 1.8$, see figure 4). Hydro-

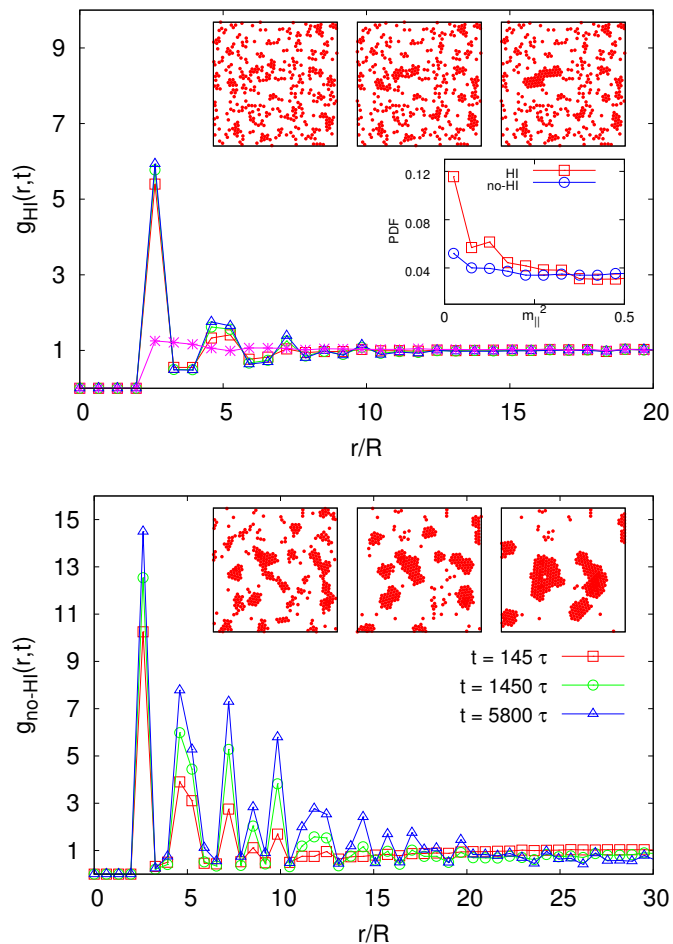


FIG. 6. RDFs for $\mu = -0.16$ at three different times and corresponding snapshots of the colloid distribution, indicating cluster formation, in a sub-system of size 256×256 , located in the center of the box. The two panels correspond to simulations with (TOP) and without (BOTTOM) hydrodynamic interactions among colloids. In the top figure also the repulsive case $\mu = +0.16$ (*) is reported for comparison. TOP PANEL INSET: PDFs of m_{\parallel}^2 , the square magnitude projection onto the $\{x, y\}$ -plane of the colloid orientations, from simulations with (HI) and without (no-HI) hydrodynamics.

dynamics hinders, then, the colloidal aggregation process. Several complex mechanisms can be conjectured to cause this phenomenon: dynamically induced effective repulsion among particles, fluid flow generated disturbances in the chemical field distribution, etc. An effect, that we could clearly identify, is an enhanced tendency of SPCs to be oriented *off-plane*, when HI are present, not only when they hit a cluster (as, e.g., in the mechanism proposed in [72]) but also for isolated particles. This may be attributed to fluid motion close to the wall, giving rise to hydrodynamic torques that rotate the particles. Actually the roto-translational dynamics of self-diffusiophoretic colloids, at and close to interfaces, is an

intricate problem [73–75]: in highly confined situations, one might indeed expect even the opposite trend (clusterisation enhancement) [72]; the argument maintains, therefore, a qualitative character. Nevertheless, the inset in the Fig. 6 (top panel) provides a quantitative insight to the picture. There, we show the PDF of the degree of alignment of the particle orientation with the bounding solid wall, $m_{\parallel}^2 = m_x^2 + m_y^2$. When HI are present, indeed, the peak of the PDF around $m_{\parallel}^2 \sim 0$ is more pronounced, *i.e.* there is a larger fraction of colloids pointing out of the plane. Accordingly, the self-propulsion speed is effectively reduced, thus limiting the *in-plane* mobility and diminishing the capability of particles to gather and clusterize. Before concluding, we would like to remind that it is still an open issue whether Janus particles can really have a homogeneous phoretic mobility; if the opposite is true, *i.e.* inhomogeneous $\mu(\mathbf{r})$ gives rise, in response to gradients of the concentration field, to *chemical* torques that can lead, themselves, to clustering inhibition [76–78]. With hydrodynamic interactions, the dynamics is, of course, even more complicated, due to the competition of these effects, and it is subject of ongoing research.

IV. CONCLUSIONS

To conclude, we have used a mesoscopic numerical model of fully resolved spherical active colloids, propelled by self-generated gradients of a scalar field (e.g. a chemical product) where the self-induced hydrodynamic flows can be accounted for. We have identified the role of the phoretic mobility as the key controlling parameter that determines two distinct dynamic regimes and the onset of a cluster phase. By means of a Voronoi tessellation we have characterized the cluster state finding that the probability distribution of sizes decays exponentially with a mean size growing linearly with the particle activity, in agreement with experimental results [9, 26]. We have quantified the profound effect that hydrodynamics plays inhibiting clustering for negative phoretic mobilities. We have identified the interplay between induced flows and particle reorientation as a possible explanation to the strong slowing down of cluster coarsening, although it remains an open question, which needs a deeper analysis, whether fluid-wall interactions dominate over particle-particle hydrodynamic correlations. This study shows that our novel numerical method is powerful and enjoys some unique features, namely the explicit description of chemical signalling, through the production and diffusion of a solute concentration field and the solvent hydrodynamics, to simulate realistic systems. Moreover, it opens the way to address the dynamics of self-propelled colloids in general geometries and also for stronger activity (larger Pe), both in isotropic and unforced situations, where aggregation can lead to the formation of active colloidal gels, or under gravity as in the experimental sedimentation setup.

ACKNOWLEDGEMENTS

We acknowledge the Spanish MINECO and Generalitat de Catalunya DURSI for financial support under the projects FIS2015-67837-P and 2014SGR-922, respectively. I.P. acknowledges *Generalitat de Catalunya* un-

der Program *Icrea Acadèmia*. This work was possible thanks to the access to MareNostrum Supercomputer at Barcelona Supercomputing Center (BSC) and also through the Partnership for Advanced Computing in Europe (PRACE).

-
- [1] M. Marchetti, J.-F. Joanny, S. Ramaswamy, T. Liverpool, J. Prost, M. Rao, and R. Simha, *Rev. Mod. Phys.* **85**, 1143 (2013).
- [2] S. Ramaswamy, *Annu. Rev. Cond. Matter Phys* **1**, 323 (2010).
- [3] E. Budrene and H. Berg, *Nature* **349**, 630 (1991).
- [4] T. Vicsek, T. Czirók, E. Ben-Jacob, I. Cohen, and O. Shochet, *Phys. Rev. Lett.* **75**, 1226 (1995).
- [5] A. Cavagna and I. Giardina, *Annu. Rec. Cond. Matter Phys.* **5**, 183 (2014).
- [6] F. Ginelli and H. Chaté, *Phys. Rev. Lett.* **105**, 1681032 (2010).
- [7] F. Peruani, A. Deutsch, and M. Bär, *Phys. Rev. E* **74**, 030904 (2006).
- [8] M. Cates, D. Marenduzzo, I. Pagonabarraga, and J. Tailleur, *Proc. Natl. Acad. Sci. USA* **107**, 11715 (2010).
- [9] I. Buttinoni, J. Biaké, F. Kümmel, H. Löwen, C. Bechinger, and T. Speck, *Phys. Rev. Lett.* **110**, 238301 (2013).
- [10] W. Paxton, K. Kistler, C. Olmeda, A. Sen, S. K. S. Angelo, Y. Cao, T. Mallouk, P. Lammert, and V. Crespi, *J. Am. Chem. Soc.* **126**, 13424 (2004).
- [11] R. Dreyfus, J. Baudry, M. Roper, M. Fermigier, H. Stone, and J. Bibette, *Nature* **437**, 862 (2005).
- [12] J. Howse, R. Jones, A. Ryan, T. Gough, R. Vafabakhsh, and R. Golestanian, *Phys. Rev. Lett.* **99**, 048102 (2007).
- [13] J. Palacci, C. Cottin-Bizonne, C. Ybert, and L. Bocquet, *Phys. Rev. Lett.* **105**, 088304 (2010).
- [14] S. Ebbens and J. Howse, *Soft Matter* **6**, 726 (2010).
- [15] L. Giomi, N. Hawley-Weld, and L. Mahadevan, *Proc. R. Soc. A* **469**, 20120637 (2013).
- [16] C. Bechinger, R. D. Leonardo, H. Löwen, C. Reichhardt, G. Volpe, and G. Volpe, *Rev. Mod. Phys.* **88**, 045006 (2016).
- [17] S. Ebbens, *Curr. Opin. Colloid Interface Sci.* **21**, 14 (2016).
- [18] A. Snezhko and I. Aranson, *Nat. Mater.* **10**, 698 (2011).
- [19] A. Demirörs, F. Eichenseher, M. Loessner, and A. Studart, *Nat. Comm.* **8**, 1872 (2017).
- [20] J. Gómez-Solano, S. Samin, C. Lozano, P. Ruedas-Batuecas, R. van Roij, and C. Bechinger, *Sci. Rep.* **7**, 14891 (2017).
- [21] M. Popescu, M. Tasinkevych, and S. Dietrich, *Europhys. Lett.* **95**, 28004 (2011).
- [22] R. Golestanian, T. Liverpool, and A. Ajdari, *Phys. Rev. Lett.* **94**, 220801 (2005).
- [23] R. Golestanian, T. Liverpool, and A. Ajdari, *New J. Phys.* **9**, 126 (2007).
- [24] M. Popescu, W. Uspal, and S. Dietrich, *Eur. Phys. J. Special Topics* **225**, 2189 (2016).
- [25] G. Rückner and R. Kapral, *Phys. Rev. Lett.* **98**, 150603 (2007).
- [26] I. Theurkauff, C. Cottin-Bizonne, J. Palacci, C. Ybert, and L. Bocquet, *Phys. Rev. Lett.* **108**, 268303 (2012).
- [27] J. Palacci, S. Sacanna, A. Steinberg, D. Pine, and P. Chaikin, *Science* **339**, 936 (2013).
- [28] F. Ginot, I. Theurkauff, F. Detcheverry, C. Ybert, and C. Cottin-Bizonne, *Nat. Comm.* **9**, 696 (2018).
- [29] C. Maggi, J. Simmechen, F. Saglimbeni, M. Dipalo, F. D. Angelis, S. Sánchez, and R. D. Leonardo, *Small* **12**, 446 (2015).
- [30] S. Succi, *The lattice Boltzmann equation for complex states of flowing matter* (Oxford University Press, 2018).
- [31] J.-C. Desplat, I. Pagonabarraga, and P. Bladon, *Comp. Phys. Comm.* **134**, 273 (2001).
- [32] K. Stratford, R. Adhikari, I. Pagonabarraga, and J.-C. Desplat, *J. Stat. Phys.* **121**, 163 (2005).
- [33] K. Stratford and I. Pagonabarraga, *Comput. Math. Appl.* **55**, 1585 (2008).
- [34] M. Swift, E. Orlandini, W. Osborn, and J. Yeomans, *Phys. Rev. E* **54**, 5041 (1996).
- [35] V. Kendon, M. Cates, I. Pagonabarraga, J.-C. Desplat, and P. Bladon, *J. Fluid Mech.* **440**, 147 (2001).
- [36] A. Ladd, *J. Fluid Mech.* **271**, 285 (1994).
- [37] A. Ladd, *J. Fluid Mech.* **271**, 311 (1994).
- [38] C. Aidun, Y. Lu, and E.-J. Ding, *J. Fluid Mech.* **373**, 287 (1998).
- [39] N.-Q. Nguyen and A. Ladd, *Phys. Rev. E* **66**, 046708 (2002).
- [40] J. Anderson, *Annu. Rev. Fluid Mech.* **21**, 61 (1989).
- [41] A. Walther and A. Müller, *Soft Matter* **4**, 663 (2008).
- [42] F. Sciortino, A. Giacometti, and G. Pastore, *Phys. Rev. Lett.* **103**, 237801 (2009).
- [43] R. Golestanian, *Phys. Rev. Lett.* **108**, 038303 (2012).
- [44] D. Lüsebrink and M. Ripoll, *J. Chem. Phys.* **136**, 084106 (2012).
- [45] M. Yang, A. Wysocki, and M. Ripoll, *Soft Matter* **10**, 6208 (2014).
- [46] J. Taktikos, V. Zaburdaev, and H. Stark, *Phys. Rev. E* **84**, 041924 (2011).
- [47] J. Taktikos, V. Zaburdaev, and H. Stark, *Phys. Rev. E* **85**, 051901 (2012).
- [48] M. McBride, *Annu. Rev. Microbiol.* **55**, 49 (2001).
- [49] F. Peruani, J. Starruß, L. Søgaard-Andersen, A. Deutsch, and M. Bär, *Phys. Rev. Lett.* **108**, 098102 (2012).
- [50] M. Popescu, S. Dietrich, M. Tasinkevych, and J. Ralston, *Eur. Phys. J. E* **31**, 351 (2010).
- [51] F. Janoschek, J. Harting, and F. Toschi, arXiv:1308.6482 (2013).
- [52] J. Brady and G. Bossis, *Annu. Rev. Fluid Mech.* **20**, 111 (1988).
- [53] E. Yariv, *Phys. Rev. Fluids* **1**, 032101(R) (2016).
- [54] A. Varma, T. Montenegro-Johnson, and S. Michelin, *Soft Matter* **14**, 7155 (2018).

- [55] Y. Fily and M. Marchetti, *Phys. Rev. Lett.* **108**, 235702 (2012).
- [56] G. Redner, M. Hagan, and A. Baskaran, *Phys. Rev. Lett.* **110**, 055701 (2013).
- [57] O. Pohl and H. Stark, *Phys. Rev. Lett.* **112**, 238303 (2014).
- [58] R. Soto and R. Golestanian, *Phys. Rev. Lett.* **112**, 068301 (2014).
- [59] F. Alarcón, C. Valeriani, and I. Pagonabarraga, *Soft Matter* **13**, 814 (2017).
- [60] G. Voronoi, *J. Reine Angew. Math.* **133**, 97 (1908).
- [61] C. Rycroft, G. Grest, J. Landry, and M. Bazant, *Phys. Rev. E* **74**, 021306 (2006).
- [62] We follow the standard procedure of embedding each particle in a d -dimensional cell whose i -th edge (face) is set to be equally distant from the reference particle and its i -th nearest neighbour.
- [63] B. Liebchen, D. Marenduzzo, I. Pagonabarraga, and M. Cates, *Phys. Rev. Lett.* **115**, 258301 (2015).
- [64] O. Pohl and H. Stark, *Eur. Phys. J. E* **38**, 93 (2015).
- [65] We set such cutoff to the value of $\Lambda = 2R + h$, h being the hard-core range of interaction.
- [66] T. Witten and L. Sander, *Phys. Rev. Lett.* **47**, 140 (1981).
- [67] P. Meakin, *Phys. Rev. Lett.* **51**, 1119 (1983).
- [68] In principle there can be a dependence on μ also of the fractal dimension d_f ; we assume here, however, that the change in μ affects only the characteristic cluster size and not its “compactness” (or fractality).
- [69] M. Popescu, W. Uspal, Z. Eskandari, M. Tasinkevych, and S. Dietrich, *Eur. Phys. J. E* **41**, 145 (2018).
- [70] P. Meakin, *Rev. Geophys.* **29**, 317 (1991).
- [71] J.-P. Hansen and I. McDonald, *Theory of simple liquids*, 3rd ed. (Elsevier, 2006).
- [72] A. Zöttl and H. Stark, *Phys. Rev. Lett.* **112**, 118101 (2014).
- [73] S. Das, A. Garg, A. Campbell, J. Howse, A. Sen, D. Velezol, R. Golestanian, and S. Ebben, *Nat. Comm.* **6**, 8999 (2015).
- [74] W. Uspal, M. Popescu, S. Dietrich, and M. Tasinkevych, *Soft Matter* **11**, 434 (2015).
- [75] A. Mozaffari, N. Sharifi-Mood, J. Koplik, and C. Maldarelli, *Phys. Fluids* **28**, 053107 (2016).
- [76] S. Saha, R. Golestanian, and S. Ramaswamy, *Phys. Rev. E* **89**, 062316 (2014).
- [77] T. Bickel, G. Zecua, and A. Wurger, *Phys. Rev. E* **89**, 050303(R) (2014).
- [78] B. Leibchen, D. Marenduzzo, and M. Cates, *Phys. Rev. Lett.* **118**, 268001 (2017).